Research Article

Journal of Environmental Nanotechnology

Sustainable Synthesis of Iron Oxide Using *Plumeria alba* Flowers: Enhanced Dye Removal and Its Antimicrobial Activity

A. Revathi[1], K. Kalaivani[2*], K. Sriram[2] and M. Venkatagiri[2]

[1]Department of Chemistry, Kongu Engineering College, Perundurai, Erode, TN, India

[2]Department of Chemical Engineering, Kongu Engineering College, Perundurai, Erode, TN, India

Received: 21.04.2025 Accepted: 29.06.2025 Published: 30.09.2025

*kalaijegu@gmail.com

ABSTRACT

This paper focuses on the green synthesis of iron oxide nanoparticles using *Plumeria alba* flower extract as a sustainable reducing agent. The method of characterizing the nanoparticles using XRD, FTIR, SEM, EDX, TGA, and UV-visible spectroscopy confirmed the crystalline structure, functional groups, morphology, elemental composition, thermal stability, and optical properties of nanoparticles. Photocatalytic studies demonstrated efficient methylene violet dye degradation under sunlight and UV light, 60 and 50 % of removal attained by UV followed by sunlight. Antimicrobial tests showed strong microbial inhibition towards positive and negative microorganisms. These outcomes show the potential of using *Plumeria alba* nanoparticles in the eco-friendly approach for environmental remediation and controlling microbes.

Keywords: Iron oxide nanoparticles; Green synthesis; Dye degradation; Photocatalysis; Environmental remediation.

1. INTRODUCTION

Water pollution is mainly caused by industrial effluents, particularly in cities where the number of industries for fabric dyeing are higher. Industries engaged in the dyeing process discharge hazardous waste products into natural waterways and rivers, thereby presenting significant environmental and public health hazards that necessitate urgent intervention. Tirupur and Erode are the hubs of fabric industry. In accordance with their established definition, dyes are characterized as ionically active, chromatic and aromatic organic compounds that demonstrate a propensity for the substrates to which they are affixed (Mathur *et al.* 2024). As an effect of their heightened capacity to absorb certain wavelengths of light preferentially, dyes exhibit a perceived coloration (Gürses *et al.* 2016). When synthetic dyes are introduced into aquatic environments, these water bodies acquire distinct chromatic attributes, which subsequently diminish the penetration of sunlight and hamper photosynthetic processes, ultimately compromising water quality. The presence of dyes additionally elevates biochemical oxygen demand (BOD) and diminishes the concentration of dissolved oxygen necessary for the sustenance of aquatic organisms, resulting in adverse effects such as toxicity, environmental pollution, and eutrophication. Furthermore, the contaminants and byproducts generated are frequently characterized by their toxicological properties, exhibiting mutagenic and carcinogenic potential (Al-Tohamy *et al.* 2014; Revathi *et al.* 2024). The conventional methodologies for wastewater treatment encompass adsorption, coagulation, and precipitation. These techniques often require an extended duration to achieve completion and generate costly secondary sludge that necessitates disposal, as noted by (Muhd *et al.* 2014)

Sustainable and environmentally conscious technologies are consistently preferred for the mitigation of environmentally hazardous pollutants. Another critical domain employed for the removal of organic dyes is nanotechnology. Nanoparticles have diminutive dimensions, organized surfaces, and unique physicochemical properties. Thus, they facilitate the development of sustainable solutions to pollution. Nanoparticles can be synthesized through numerous methodologies. Iron oxide nanoparticles can be synthesized in diverse morphologies (Ajinkya *et al.* 2020). The green synthesis of nanostructures is cost-effective, uncomplicated, and ecologically friendly (Mathur *et al.* 2024). It has been documented that these materials possess potential biotechnological applications. The attributes of biocompatibility, cost-effectiveness, favourable magnetic properties, ease of surface modification, elevated recovery rates, substantial porosity, increased density, remarkable stability, and an extensive surface area facilitate a significant number of adsorption sites that characterize this phenomenon associated with iron oxide (Campos *et al.* 2015). Iron oxide has gained considerable attention from numerous researchers on account of its unique chemical and

biological characteristics, which can be attributed to its inherent morphology (Nene *et al.* 2016).

Methyl violet is widely used in the textile industries. Tirupur and Erode districts are the two main areas where there is an enormous growth in textile sector in recent times but the improper disposal of this dye leads to significant environmental issues. In order to overcome this issue, the photocatalytic degradation technique is adopted widely in recent times as it shows excellent degradation properties when compared with other techniques like chemical oxidation, adsorption, coagulation etc

The characterization of iron oxide nanoparticles, commonly designated as Fe_2O_3-NPs, was rigorously performed utilizing a range of advanced analytical methodologies, encompassing but not confined to ultraviolet-visible (UV–vis) spectroscopy, scanning electron microscopy (SEM), thermogravimetric analysis (TGA), Fourier-transform infrared (FTIR) spectroscopy, and X-ray diffraction (XRD) analysis, along with antibacterial evaluation (well diffusion method), each of which furnished essential insights into the structural and functional characteristics of the nanoparticles. Furthermore, these Fe_2O_3-NPs were utilized in a comparative study designed to clarify their effectiveness in the photocatalytic decolorization of diverse dye contaminants, particularly concentrating on the degradation of violet, while also demonstrating antibacterial properties by suppressing the proliferation of gram-positive followed by gram-negative bacteria, thus contributing to the expansive domain of environmental remediation and sustainability (Salem and Fouda, 2021).

2. MATERIALS AND METHODS

2.1 Collection of Flowers

The frangipani (*Plumeria alba*) flowers were collected from the trees in and around Perundurai, Tamil Nadu, India. All the chemicals used were of laboratory grade with 99% purity. Deionized water was used for all experiments and all assays were performed in triplicates (Nam *et al*. 2009).

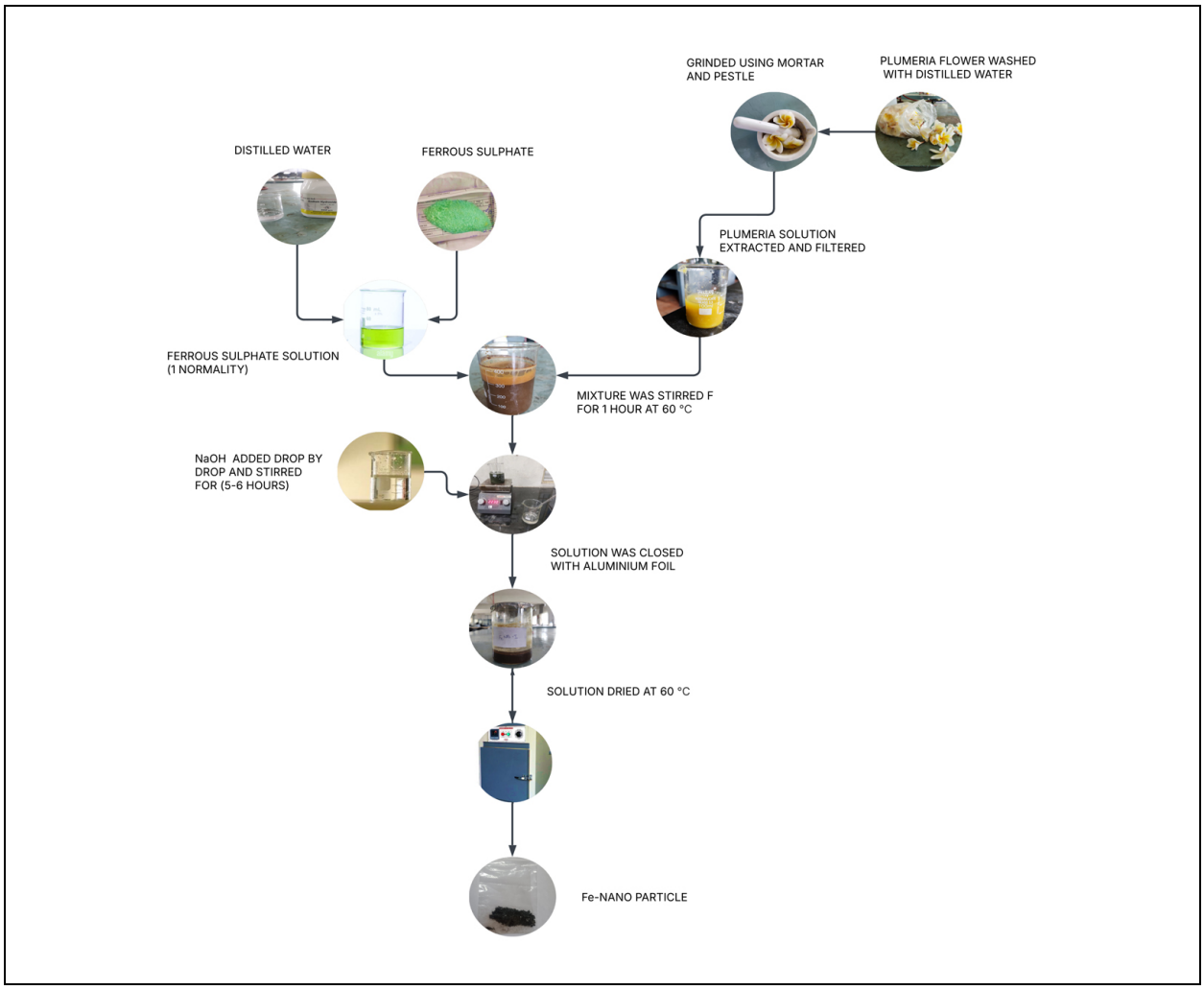


Fig. 1: Iron oxide NPs preparation method

Fresh *Plumeria alba* flowers were systematically harvested and meticulously rinsed to eliminate any particulate matter or contaminants using tap water. Subsequently, any residual moisture was allowed to evaporate at room temperature. Following this, 10 g of the flowers was accurately measured and coarsely pulverized utilizing a pestle and mortar. It was taken in a conical flask along with 100 mL of distilled water. After subjecting the solution to a heating process at 40 ℃ for a duration of one hour, Whatman No. 1 filter paper was employed for the filtration process (Pereira and Alves, 2012).

2.2 Green Synthesize of Iron Oxide Nanoparticles

1 M Ferrous sulphate heptahydrate [$FeSO_4.7H_2O$; molecular weight 278 g/mol] was solubilized in 100 mL of distilled water and subjected to stirring for a duration of 1 hour. In a similar manner, 1 M NaOH (molecular weight 40 g/mol) pellet was dissolved in 100 mL of double distilled water then stirring for approximately 1 hour. The flower extract was subsequently introduced into the ferrous sulphate solution, to which the NaOH solution was incrementally added dropwise to the prior mixture, followed by an additional mixing period of 1 hour. Thereafter, the mixture was agitated for an extended duration of 4 to 5 hours at a constant rpm. A brown precipitate was observed, signifying the formation of iron oxide nanoparticles as shown respectively in Fig. 1. The pellet was removed after the precipitate was isolated from the solution by keeping the solution in an oven for 2 days at 80℃.To eliminate any contaminants, the pellet underwent three wash cycles utilizing distilled water. Ultimately, the pellet was desiccated in an oven at 75 ℃ for 1 hour. For subsequent investigations, the brown iron oxide nanoparticle powder was stored.

2.3 Characterization of Iron oxide Nanoparticles

The synthesized nanoparticles underwent comprehensive characterization utilizing UV-Visible spectroscopy, Fourier Transform Infrared (FTIR) spectroscopy and X-ray diffraction. To confirm the synthesis of iron oxide nanoparticles, UV-visible absorption spectrum was obtained using a DB20S UV Spectrophotometer. By employing the KBr pellet technique, we successfully acquired the FTIR spectrum (Shimadzu) of iron oxide nanoparticles synthesized using *Plumeria alba* flower extract (Mathur *et al.* 2024; Revathi *et al.* 2024). The crystalline structure of the prepared iron oxide nanoparticles, Fe_2O_3-NPs, was evaluated in detail using X-ray diffraction. More specifically, X-Ray diffraction patterns were obtained systematically (XRD 6000 series advanced apparatus). The Debye-Scherrer equation was used to calculate the average crystalline dimension of iron oxide nanoparticles like Fe_2O_3-NPs as follows

$$D = {k\lambda}/{\beta \cos\theta} \quad \ldots (1)$$

where, D is the average size in nm, k is the Scherrer constant, λ is the X-ray wavelength, β = full width at half maximum, and θ is the Bragg diffraction angle.

2.4 Photocatalytic Degradation of Methyl Violet

The synthesized iron oxide nanoparticles were tested for their photocatalytic ability to degrade methyl violet (MV) dye. The results revealed that they are capable of efficiently bleaching the applied dye as aquatic pollutant. Experimental study was carried out on a sunny day (the temperature was between 30 and 34℃) in the month of August.

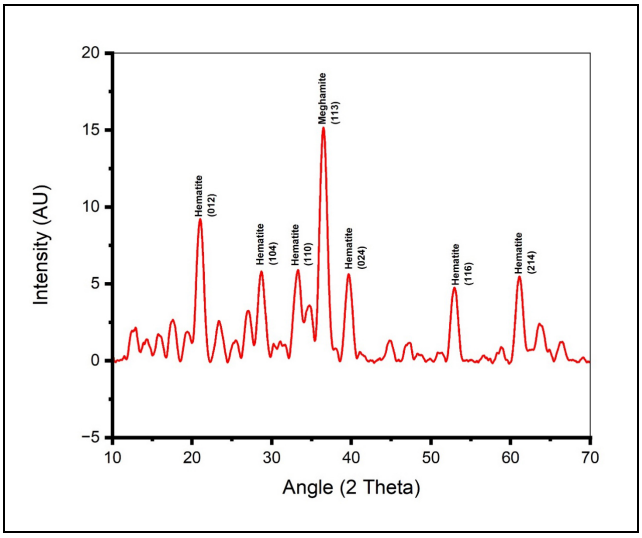


Fig. 2: X-ray Diffraction spectrum

The test sample was prepared with 50 mL of distilled water in a beaker with MV dye. Each beaker was then amended with 25 mg of iron oxide nanoparticles. The mixtures were subjected to photocatalytic degradation through direct solar radiation. In parallel, two control groups were also set up: (i) Methyl violet dye solution with nanoparticles exposed to sunlight and (ii) Methyl violet dye solution with nanoparticles in the presence of UV radiation. The degradation of pollutants was visualized at fixed interval time along with zinc oxide and the residual concentration of dye was calculated by measuring absorbance of pollutants at resonance wavelength (Mathur *et al.* 2024).

3. RESULTS and DISCUSSION

3.1 XRD Analysis

The structure of green synthesized *Plumeria alba* iron oxide nanoparticles was examined by using XRD (Bruker D8 Advance). The comparison of the obtained XRD results was done with the help of Joint Committee on Powder Diffraction Standards (JCPDS) X-

ray data file. The XRD spectrum of synthesized iron oxide nanoparticles is shown in Fig. 2. The major XRD peak is observed at 2θ = 33.3°, while the second major peak is recorded at 2θ = 36.6°. The peak at 36.6° is due to the presence of γ-Fe_2O_3 phase matched with the standard JCPDS data (card no. 19-0629) and all other peaks are of α-Fe_2O_3 phase matched with standard JCPDS data (card nos. 13-534 and 24-72). Thus, α-Fe_2O_3 (hematite phase) is the dominant phase compared with γ -Fe_2O_4 (maghemite phase). The Scherrer relation confirms the crystallite size of the nanoparticles based on the broadening of XRD peaks (Kayani *et al.* 2014).

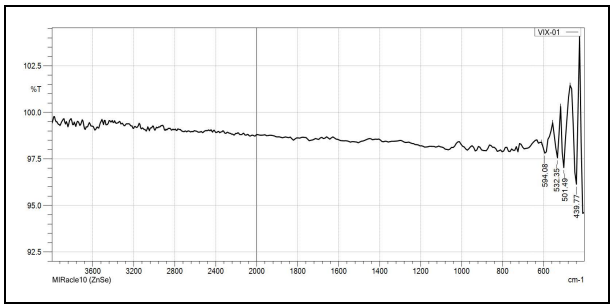


Fig. 3: FT-IR spectrum

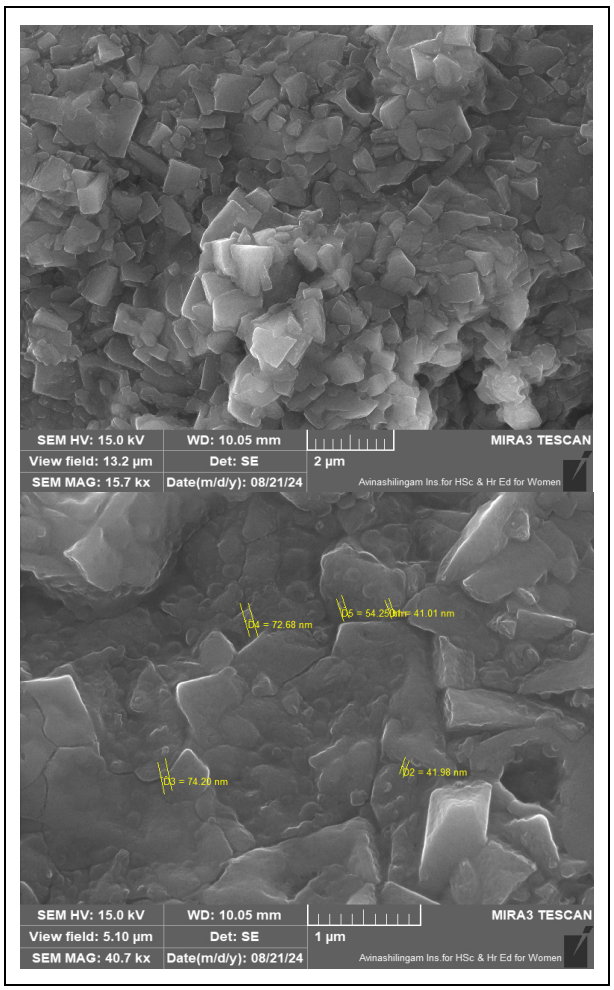


Fig. 4: SEM images of iron oxide NPs (SEM A, SEM B)

3.2 FT-IR Analysis

Fourier Transform Infrared Spectroscopy was used to identify specific functional groups present in the *Plumeria alba* plant extract (Fig. 3). The peak/bands determined were: a characteristic (Fe-O) vibration region at 439.77 cm^{-1}, magnetite stretching at 501.49 cm-1, hematite stretching at 532.35 cm^{-1} and Fe_2O_4 stretching at 594.08 cm^{-1} confirming that the nanoparticles formed are likely to be iron oxide nanoparticles.

3.3 FE-SEM with EDX Analysis

The morphological features and elemental constituents of the synthesized iron oxide nanoparticles were characterized through SEM and EDX. The SEM images of the synthesized nanoparticles exhibited spherical morphology predominantly (Fig. 4). The variations observed may be ascribed to the presence of distinct phytochemical compositions within the plant, which likely resulted in the varied formation of spherical and rod-shaped Fe_2O_4 nanoparticles. The pore structure observed ranged from 41.01 nm to 74.20 nm and the visible high degree of porosity suggested the adsorption capacity. The different pore texture increases the adsorption of the iron oxide nanoparticles. Furthermore, the EDX analysis was conducted to examine the elemental composition of the prepared iron oxide sample. Fig. 5 clearly indicates the presence of the K-α at 7.05 keV due to presence of Fe atoms in the nanoparticle and K-α line at 0.6 keV resulted from the O atoms (Bhuiyan *et al.* 2020).

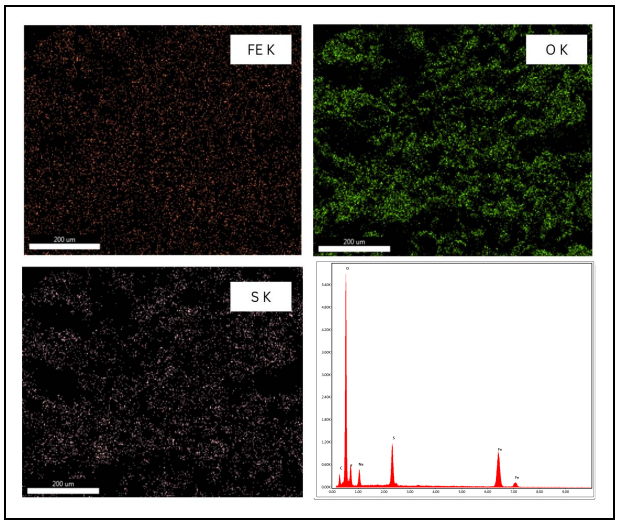


Fig. 5: EDX images of nanoparticles

The mass present in terms of percentage under the irradiated area is 44.85%, 33.64% and 5.88%, for iron, oxygen and less carbon content, respectively (Fig. 5). The presence of carbon particles is attributed to organic components from the *Plumeria alba* plant extract adsorbed onto the nanoparticle surface. Additionally, chlorine impurities observed during the synthesis of

Fe_2O_3 nanoparticles from ferric chloride are consistent with findings reported by Bhuiyan *et al*. (2020).

3.4 Thermogravimetric Analysis

Thermogravimetric analysis was done to evaluate the decomposition temperature, thermal stability of the synthesised nanoparticle and also the rate of decomposition of the iron oxide nanoparticles (Bhuiyan *et al.* 2020). The temperature range was from 0 to 900 ℃. In the first step of thermal analysis displayed, the sample attained weight stability at low temperatures (0–200 ℃) with no significant loss in mass indicating low volatility and hygroscopic nature of the compound (Fig. 6). The first visible decrease of 11.9% takes place between 200 and 300 ℃, which could be explained by the vaporization of volatile compounds or moisture loss due to temperature increase. A 17.1% of weight loss is observed between 300 ℃ and 500 ℃, indicating further degradation. The weight loss can be associated with the degradation of organic components or to the pyrolytic decomposition of certain constituents in the material. The occurrence of functional groups can lead to mass loss by pyrolysis. The curve stabilizes at around 500 ℃, representing intermediate stability with a weight loss of around 2.7%. Normally, this plateau indicates that the material is stable in its phase, likely consisting of thermally resistant inorganic residues or char. As the temperature approaches 900 ℃, there is a gradual loss of mass, ending in a final residual mass of approximately 5.0%. This final weight loss reflects the decomposition of residual inorganic compounds or further thermal degradation of the charred material (Beheshtkhoo *et al*. 2018).

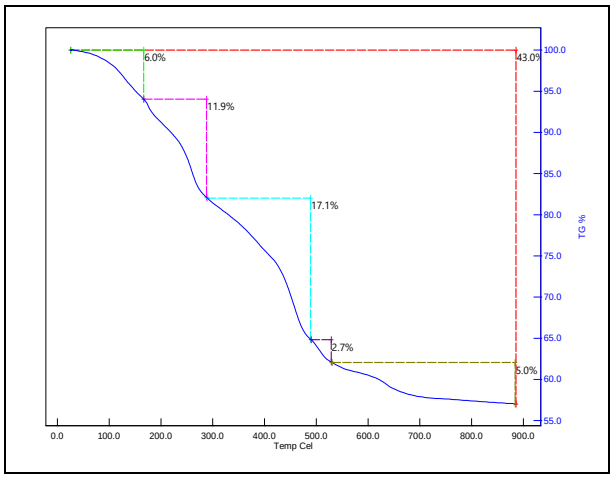


Fig. 6: Thermogravimetric analysis plot

3.5 UV–visible Analysis

The degradation of methyl violet dye in UV and sunlight for Fe_2O_3-NPs was used to assess photocatalytic activity for various time intervals from 0 to 120 minutes (Fig. 7). The UV–visible spectroscopy was undertaken to quantify the decrease in concentration of dye by monitoring the degradation efficiency over a time period. From the results of absorbance *vs* wavelength, a clear peak at 580 nm is noticed, which is the peak absorbance point for Fe_2O_3-NPs. The absorbance is high at the initial time of 0 minutes then gradually decreases as time progresses and at 120 minutes absorbance becomes very low for the dye degradation both under UV lamp and sunlight (Minisha *et al.* 2023).

In Sunlight: High degradation rate of the nanoparticles was noted, which showed high photocatalytic activity. For example, the degradation efficiency was as high as 60% in exposure range of 120 minutes, which can be observed from the degradation% (*vs*) time plot under sunlight, shown in Fig. 7 (A, B). This increased degradation is due to the band gap of the nanoparticles (2.2 eV), which is adequate for absorbing visible light range (Kim *et al*. 2016).

In UV Light: Degradation rate under UV light was almost the same as under sunlight (Fig. 7 C, D). However, a slight reduction in degradation is noted. This may be due to the closed environment for the UV light apparatus and the band gap which is suitable for visible light range. The degradation rate is only slightly low considering the influence of nature of the dye species. The degradation percentage was 54% after it had been exposed for around 120 mins. Degradation percentage of other materials and dye pollutants are shown in Table 1.

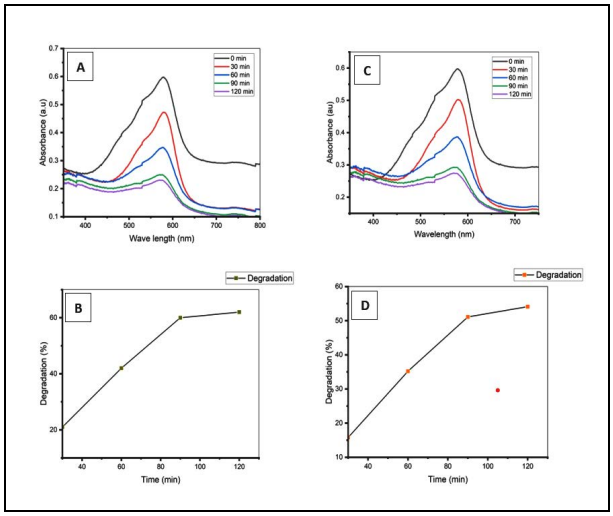


Fig. 7: UV-visible absorbance spectra and rate of dye degradation for methyl violet

Tauc plot, dye degradation under sunlight and UV light, as well as the rate of adsorption data are crucial in understanding the behaviour of the nanoparticles. Optical band gap of Fe_2O_3-NPs is determined by Tauc Plot. A plot of $(E.\alpha)^2$ versus the photon energy (E) depicts a steep, almost vertical rise at approximately 2.2 eV where strong absorption begins. The straight segment of the curve extrapolated to the energy axis intersects at

about 2.2 eV which corresponds to the optical band gap energy for the dye removal (Fig. 8). The reaction mechanism is shown in Fig. 9.

The results of a UV–visible analysis and Tauc plot as well as photocatalytic dye degradation studies indicate that the iron oxide nanoparticles are excellent photocatalysts and are suitable for environmental remediation as band gap energy of ~2.2eV allows organic pollutants to be degraded through sunlight and under UV light. The high adsorption rate and effective degradation upon UV light activation make the iron oxide nanoparticles promising in environmental applications (Li *et al.* 2015a).

Table 1. Degradation percentage of other materials and dyes

Plant Material	MNPs	Size and Shape	Organic Dyes	Catalytic Reagents/ Sunlight	Degradation (%) and Rate in min^{-1}	Ref.
Ruellia tuberose leaf	FeO-NPs	52.78 nm, hexagonal nanorods with agglomeration	Crystal violet	Sunlight	80%	(Vasantharaj *et al.* 2022)
Hibiscus sabdariffa flower	FeO-NPs	10–100 nm, spherical	CR	UV-light	96.1%, 100 mM, pH 4	(Alshehri *et al.* 2017)
Pisum sativum peel	Fe_3O_4-NPs	20–30 nm, spherical	MO	Adsorption	96.2%, 100 mg/L	(Prasad *et al.* 2017)
Plantago major leaf	FeO-NPs	FeO-NPs	MO 4.6–30.6 nm, spherical	H_2O_2	83.33%	(Lohrasbi *et al.* 2019)
Wedelia urticifolia leaf	FeO-NPs	70 nm, rod	MB	Sunlight	0.3299 min^{-1}	(Rather *et al.* 2020)
Amaranthus spinosus leaf	FeO-NPs	91 nm, rhombo-hedral	MO and MB	Sunlight	75% and 69%	(Muthukumar and Matheswaran, 2015)
Green tea leaf	FeNPs	130–270 nm, aggregated	MB	$NaBH_4$	0.0404 min^{-1}	(Lin *et al.* 2015)
Grape leaf	nZVI/Fe⁰NPs	18–30 nm	Orange II	High temperature	>92%	(Ge *et al.* 2015)
Cynara cardunculus leaf	Fe_3O_4-NPs	13.5 nm, semi-spherical, aggregated	MB	Adsorption	>90%	(Li *et al.* 2019b)
Green, Oolong, and Black teas	FeNPs	40–50 nm	MG	Adsorption	81.6%, 75.6%, and 67.1%	(Habibi, 2014)
Andean blackberry leaf	Fe_3O_4-NPs	54.5 ±/− 24.6 nm, spherical	MB, CR, MO	Sunlight	0.0105475, 0.0043240, and 0.002893 min^{-1}	(Haog *et al.* 2009)
Camellia sinensis leaf	nZVI/Fe⁰NPs	5 to 15 nm, spherical	Bromothymol blue	H_2O_2	0.1447 min^{-1}	(Kumar *et al.* 2016)

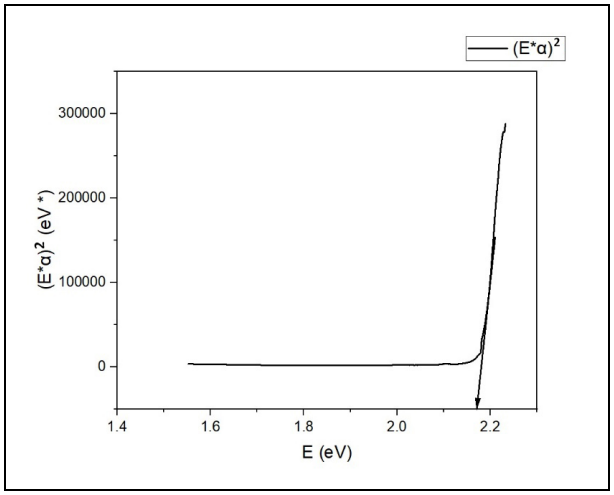


Fig. 8: Tauc plot of iron oxide NPs

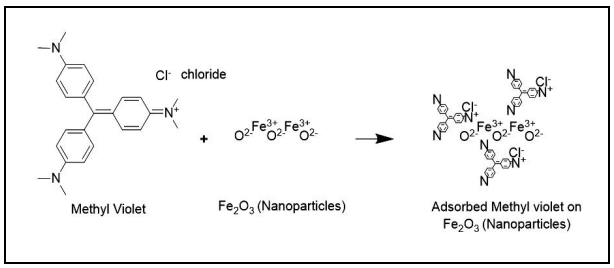


Fig. 9: Reaction of methyl violet dye and Fe_2O_3 NPs

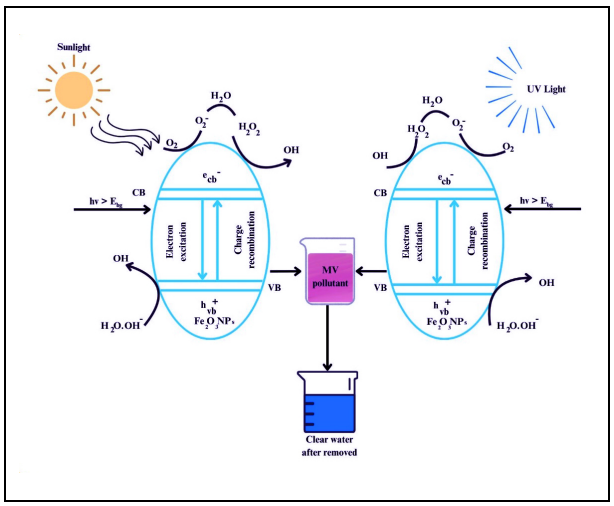


Fig. 10: Schematic illustration of methyl violet dye degradation

Potential degradation of methyl violet dye under UV and sunlight is shown in Fig. 10.

The –N=N– (azo) bonds found in dyes like methyl orange (MO) are specifically targeted by iron nanoparticles (Fe NPs), which are important in the breakdown of organic dyes. Prasad C. et al. (2017) claim that iron nanoparticles work very well in sunshine and ultraviolet light, assisting in the breakage of these azo bonds and causing dye degradation. The procedure is effective and eco-friendly because the photoactivation of Fe NPs produces reactive species such hydroxyl radicals (•OH), which target and destroy the dye's molecular structure. Because of their –N=N– connections, which become less stable when exposed to light and Fe NPs, azo dyes, such as MO, are particularly prone to deterioration. These nanoparticles actively take part in chemical reactions that break down the dye into less toxic, simpler chemicals in addition to adsorbing the dye molecules onto their surface.

Iron nanoparticles were also used to remove methylene blue (MB) dye, according to Rather et al. (2020). They investigated the impact of changing the duration of contact between the dye and the adsorbent and discovered that greater removal effectiveness resulted from longer contact durations. The study also looked at the iron nanoparticles' reusability and found that they continued to function well across several cycles. Remarkably, MB dye was degraded by up to 99%, mostly as a result of hydroxyl radicals attacking the dye molecules.

All things considered, iron nanoparticles are a dual-purpose substance that support dye adsorption as well as photocatalytic degradation, which makes them extremely promising for wastewater treatment applications.

3.6 Anti-bacterial Activity

Stock cultures were preserved at the temperature of 4°C on nutrient agar medium. Active cultures were prepared by transferring a loopful of cells into 50 mL test tubes with nutrient broth and incubated with agitation at 37 °C for 24 hours (Prabu *et al.* 2017). The suspension of each organism was subsequently streaked onto nutrient agar, followed by incubation. The antibacterial activity was assessed *via* the well diffusion method, where nanoparticle extracts were introduced into wells, incubated, and the inhibition zones were measured in mm (Logeswari *et al.* 2015).

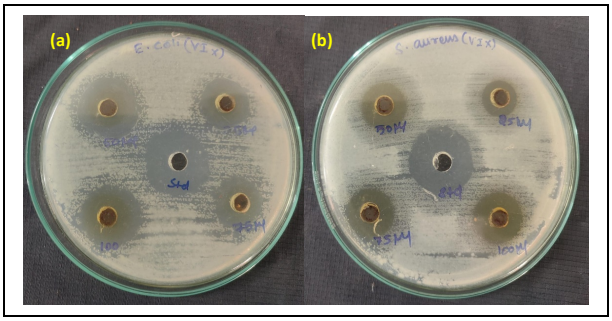


Fig. 11: Well diffusion result of *E. coli* (a) and *S. aureus* (b)

The antibacterial activity was assessed using the agar diffusion technique as per standard method depicted in Fig. 11. The results are summarized in Table 2.

Table 2. Concentration of organism and inhibition diameter data of *E. coli* and *S. aureus*

Concentration (µL)	Zone of Inhibition for *E. coli* (mm)	Zone of Inhibition for *S. aureus* (mm)
25	5	3
50	8	6
75	9	8
100	12	10
E. coli and *S. aureus*	15	15

Fig. 12 shows the plot of inhibitory concentration (µL) of NPs against zone of inhibition (mm) for Gram-positive and Gram-negative bacteria.

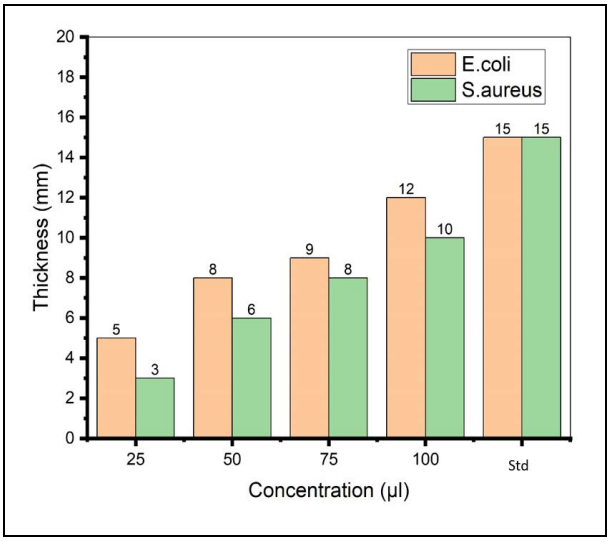


Fig. 12: Plot of iron oxide nanoparticle concentration *vs.* zone of inhibition

4. CONCLUSION

Green synthesis method is used for the synthesis of the iron oxide nanoparticle with *Plumeria alba* flower extract. Their structural and optical properties were analysed with various techniques. X-ray diffraction showed the crystalline nature of nanoparticles. FT-IR spectrum showed the presence of Fe-O bonds indicating the formation of iron nanoparticles, while FE-SEM revealed the surface morphology and pore size of the NPs. The results of EDX study showed the composition of iron oxide NPs, with Fe as its main component and TGA analysis showed the thermal stability of the particles. Photocatalytic studies done for different light sources with methyl violet dye showed dye degradation (54% for UV light and 60% for sunlight) in 120 minutes. Antimicrobial studies show the NPs ability to inhibit microbial growth of Gram-positive and Gram-negative bacteria. All the results show promising performance of the iron oxide NPs and their potential in dye removal and antibacterial activity. Thus, they can be used for environmental remedy and other related applications.

FUNDING

This research received no specific grant from any funding agency in the public, commercial, or not-for-profit sectors.

CONFLICTS OF INTEREST

The authors declare that there is no conflict of interest.

COPYRIGHT

This article is an open-access article distributed under the terms and conditions of the Creative Commons Attribution (CC BY) license (http://creativecommons.org/licenses/by/4.0/).

REFERENCE

Ajinkya, N., Yu, X., Kaithal, P., Luo, H., Somani, P. and Ramakrishna, S., Magnetic Iron Oxide nanoparticle (IONP) Synthesis to Applications, Present and Future, *Mater.*, 13(20), 4644(2020). https://doi.org/10.3390/ma13204644

Alshehri, A., Malik, M. A., Khan, Z., Al-Thabaiti, S. A. and Hasan, N., Biofabrication of Fe nanoparticles in aqueous extract of Hibiscus sabdariffa with enhanced photocatalytic activities, *RSC Adv.,* 7(40), 25149–25159(2017). https://doi.org/10.1039/C7RA01251A

Al-Tohamy, R., Ali, S. S., Li, F., Okasha, K. M., Mahmoud, Y. A. G., Elsamahy, T., Jiao, H., Fu, Y. and Sun, J., A critical review on the treatment of dye-containing wastewater: Ecotoxicological and health concerns of textile dyes and possible remediation approaches for environmental safety, *Ecotoxicol. Environ. Saf.,* 231, 113160(2022). https://doi.org/10.1016/j.ecoenv.2021.113160

Beheshtkhoo, N., Kouhbanani, M. A. J., Savardashtaki, A., Amani, A. M. and Taghizadeh, S., Green synthesis of iron oxide nanoparticles by aqueous leaf extract of *Daphne mezereum* as a novel dye removing material, *Appl. Phys. A*, 124, 363(2018). https://doi.org/10.1007/s00339-018-1782-3

Gürses, A., Açıkyıldız, M., Güneş, K. and Gürses, M. S., Dyes and Pigments: Their Structure and Properties,. *Springer, Cham.*, 13–29 (2016). https://doi.org/10.1007/978-3-319-33892-7_2

Bhuiyan, M. S. H., Miah, M. Y., Paul, S. C., Aka, T. D., Saha, O., Rahaman, M. M., Sharif, Md. J. I., Habiba, O. and Ashaduzzaman, M., Green synthesis of Iron oxide nanoparticle using Carica papaya leaf extract: application for photocatalytic degradation of remazol yellow RR dye and antibacterial activity, *Heliyon.*, 6(8), e04603(2020). https://doi.org/10.1016/j.heliyon.2020.e04603

Ge, H., Tang, G., Hu, W.-Z., Wang, B. B., Pan, Y., Song, L. and Hu, Y., Aluminum hypophosphite microencapsulated to improve its safety and application to flame retardant polyamide 6, *J. Hazard Mater.*, 294, 186–194(2015). https://doi.org/10.1016/j.jhazmat.2015.04.002

Geoprincy, G., Saravanan, P., Gandhi, N. N. and Renganathan, S., A Novel Approach for Studying the Combined Antimicrobial Effects of Silver Nanoparticles and Antibiotics Through Agar Over Layer Method and Disk Diffusion Method, *Digest J. Nanomater. Biostruct.*, 6(4), 1557-1565(2011).

Habibi, N., Preparation of biocompatible magnetite-carboxymethyl cellulose nanocomposite: Characterization of nanocomposite by FTIR, XRD, FESEM and TEM, *Spectrochim. Acta. A. Mol. Biomol. Spectrosc.*, 131, 55–58(2014). https://doi.org/10.1016/j.saa.2014.04.039

Kim, H. S., Seo, Y. S., Kim, K., Han, J. W., Park, Y. and Cho, S., Concentration Effect of Reducing Agents on Green Synthesis of Gold Nanoparticles: Size, Morphology, and Growth Mechanism, *Nanoscale Res. Lett.*, 11, 1-9 (2016). https://doi.org/10.1186/s11671-016-1393-x

Kumar, B., Smita, K., Cumbal, L., Debut, A., Galeas, S. and Guerrero, V. H., Phytosynthesis and photocatalytic activity of magnetite (Fe3O4) nanoparticles using the Andean blackberry leaf,, *Mater. Chem. Phys.*, 179, 310-315(2016). https://doi.org/10.1016/j.matchemphys.2016.05.045

Li, L. H., Xiao, J., Liu, P. and Yang, G. W., Super adsorption capability from amorphousization of metal oxide nanoparticles for dye removal, *Sci. Rep.*, 5(1), 9028(2015a). https://doi.org/10.1038/srep09028

Li, Q., An, M. and Li, D., In situ growth of ZnO nanowire film on nanocrystalline zinc electrodeposit via a low-temperature hydrothermal reaction, *Results. Phys.*, 12, 1446–1449(2019b). https://doi.org/10.1016/j.rinp.2019.01.040

Lin, J., Weng, X., Jin, X., Megharaj, M., Naidu, R. and Chen, Z., Reactivity of iron-based nanoparticles by green synthesis under various atmospheres and their removal mechanism of methylene blue, *RSC. Adv.*, 5(87), 70874–70882(2015). https://doi.org/10.1039/C5RA10629J

Logeswari, P., Silambarasan, S. and Abraham, J., Synthesis of silver nanoparticles using plants extract and analysis of their antimicrobial property, *J. Saudi. Chem. Soc.*, 19(3), 311–317(2015). https://doi.org/10.1016/j.jscs.2012.04.007

Lohrasbi, S., Kouhbanani, M. A. J., Beheshtkhoo, N., Ghasemi, Y., Amani, A. M. and Taghizadeh, S., Green synthesis of iron nanoparticles using plantago major leaf extract and their application as a catalyst for the decolorization of azo dye, *BioNanoSci.*, 9(2), 317-322(2019). https://doi.org/10.1007/s12668-019-0596-x

Mathur, S., Gautam, V., Kumari, S. and Mishra, P., Photocatalytic Degradation of Organic Dye Pollutants Using ZnO Nanoparticles Synthesized from Plumeria alba L. Leaf Extract, *SSR Inst. Int. J. Life Sci.*, 10(1), 3734–3742(2024). https://doi.org/10.21276/SSR-IIJLS.2024.10.1.42

Minisha, S., Johnson, J., Mohammad, W. S., Gupta, J. K., Aftab, S., Siddiqui, M. R. and Lai, W. -C., Synthesis and Characterizations of Fe-Doped NiO Nanoparticles and Their Potential Photocatalytic Dye Degradation Activities, *Sustainability.*, 15(19), 14552(2023). https://doi.org/10.3390/su151914552

Muhd, J. N., Bagheri, S. and Bee, A. H. S., Recent Advances in Heterogeneous Photocatalytic Decolorization of Synthetic Dyes, *Sci. World. J.*, 2014, 1-25(2014). https://doi.org/10.1155/2014/692307

Muthukumar, H. and Matheswaran, M., Amaranthus spinosus Leaf Extract Mediated FeO Nanoparticles: Physicochemical Traits, Photocatalytic and Antioxidant Activity, *ACS Sustainable Chem. Eng.*, 3(12), 3149-3156(2015). https://doi.org/10.1021/acssuschemeng.5b00722

Nam, J., Won, N., Jin, H., Chung, H. and Kim, S., pH-responsive assembly of gold nanoparticles into nanoconcave superstructures with enhanced optical properties, *J. Am. Chem. Soc.*, 131(38), 13639–13645(2009). https://doi.org/10.1021/ja9022229

Nene, A. G., Takahashi, M., Wakita, K. and Umeno, M., Size Controlled Synthesis of Fe_3O_4 Nanoparticles by Ascorbic Acid Mediated Reduction of $Fe(acac)_3$ without Using Capping Agent, *J. Nano. Res.*, 40, 8-19(2016). https://doi.org/10.4028/www.scientific.net/JNanoR.40.8

Prasad, C., Yuvaraja, G. and Venkateswarlu, P., Biogenic synthesis of Fe_3O_4 magnetic nanoparticles using Pisum sativum peels extract and its effect on magnetic and Methyl orange dye degradation studies, *J. Magn. Magn. Mater.*, 424, 376-381(2017). https://doi.org/10.1016/j.jmmm.2016.10.084

Pereira, L. and Alves, M., Dyes Environmental Impact and Remediation, *Env. Protect. Strategies Sustainable Develop.*, 111–162 (2012). https://doi.org/10.1007/978-94-007-1591-2_4

Rather, M. Y. and Sundarapandian, S., Magnetic iron oxide nanorod synthesis by *Wedelia urticifolia* (Blume) DC. leaf extract for methylene blue dye degradation, *Appl. Nanosci.*, 10, 2219-2227(2020). https://doi.org/10.1007/s13204-020-01366-2

Roy, S. D., Das, K. C. and Dhar, S. S., Conventional to green synthesis of magnetic iron oxide nanoparticles; *Inorg. Chem. Commun.,* 134, 109050(2021). https://doi.org/10.1016/j.inoche.2021.109050

Salem, S. S. and Fouda, A., Green Synthesis of Metallic Nanoparticles and Their Prospective Biotechnological Applications: an Overview, *Biol. Trace. Elem. Res.*, 199(1), 344–370(2021). https://doi.org/10.1007/s12011-020-02138-3

Suganya, R., Revathi, A., Sudha, D., Sivaprakash, V. and Kumar, E., Evaluation of structural, optical properties and photocatalytic activity of Ag2O coated ZnO nanoparticles, *J. Mater. Sci. Mater. Electron.,* 33, 23224-23235(2022). https://doi.org/10.1007/s10854-022-09086-9

Vasantharaj, S., Sathiyavimal, S., Senthilkumar, P., Lewis, O. F. and Pugazhendhi, A., Biosynthesis of Iron oxide nanoparticles using leaf extract of Ruellia tuberosa: Antimicrobial properties and their applications in photocatalytic degradation, *J. Photochem. Photobiol. Biol.,* 192, 74-82(2019). https://doi.org/10.1016/j.jphotobiol.2018.12.025